The versatility of asymmetric aminoethyl-tetrazines in bioorthogonal chemistry

Sarris, A.

Chapter 6: Fluorogenic Bifunctional *Trans*-Cyclooctenes as Efficient Tools for Investigating Click to Release Kinetics

Introduction

The inverse electron demand Diels-Alder (IEDDA)-pyridazine elimination tandem reaction can be used to release allylic substituents from *trans*-cyclooctene (TCO) following a reaction with tetrazines (**chapter 5**). While the fluorogenic reporter TCO-coumarin (compound **28**, **chapter 5**) is a very useful tool to identify effective tetrazines for this elimination reaction, the results may not be an accurate fit for the actual release rates of (non-conjugated) aliphatic primary amines (often the target of TCO-caging in biological experiments). No reliable method has been reported to directly measure the true kinetic parameters of the cycloaddition and release steps in the click-to-release reaction of tetrazines with TCO-caged aliphatic primary amines. To date, by using indirect LC-MS analysis[1-2] (at non-physiological pH or non-physiological eluent), or by releasing non-aliphatic functional groups[1, 3], kinetic parameters have been obtained. Whilst being informative, these results may not translate well to the true kinetic parameters for click-to-release reactions of tetrazines with TCO-caged aliphatic primary amines in biological environments.

In this chapter, to circumvent limitations caused by indirect, non-physiological, or non-aliphatic conditions, fluorogenic probes **2** and **3** were designed using bifunctional *trans*-cyclooctene[4] (biTCO) and a FRET-pair based on the fluorophore EDANS and quencher DABCYL (**Scheme 1**). The resulting probes allow the direct approximation of IEDDA (K_{IEDDA}) and release ($K_{release}$) rate constants of TCO-caged primary aliphatic amines in a 96-well plate reader format, thereby representing the first tool to study click-to-release rates for TCO-caged primary aliphatic amines.

Design

The first aim of the research described in this chapter was to calculate the kinetic properties of tetrazines reacting with a bifunctional TCOs (as opposed to monofunctional TCOs). For this potent tetrazines from literature were identified, such as dimethyl tetrazine **4**, carboxyethyl modified tetrazines **7** and **8**, aminoethyl modified tetrazines **6**, **11** and **14** and hydroxyethyl modified tetrazine **16**. The ground state and the transition state (TS) energies were calculated for both reactions (**Figure 1**). The DFT calculations showed that, for these tetrazines, the IEDDA reaction is slower when reacting with bifunctional TCO compared to monofunctional TCO. The relative reactivity differences between individual tetrazines were similar for both TCOs and depended on the functional groups attached to the tetrazine core. Compared to tetrazine **4**, carboxyethyl functionality (tetrazines **7**-**8**) increased the TS energy, aminoethyl functionality (tetrazines **6**, **11**, **14**) lowered the TS energy due to

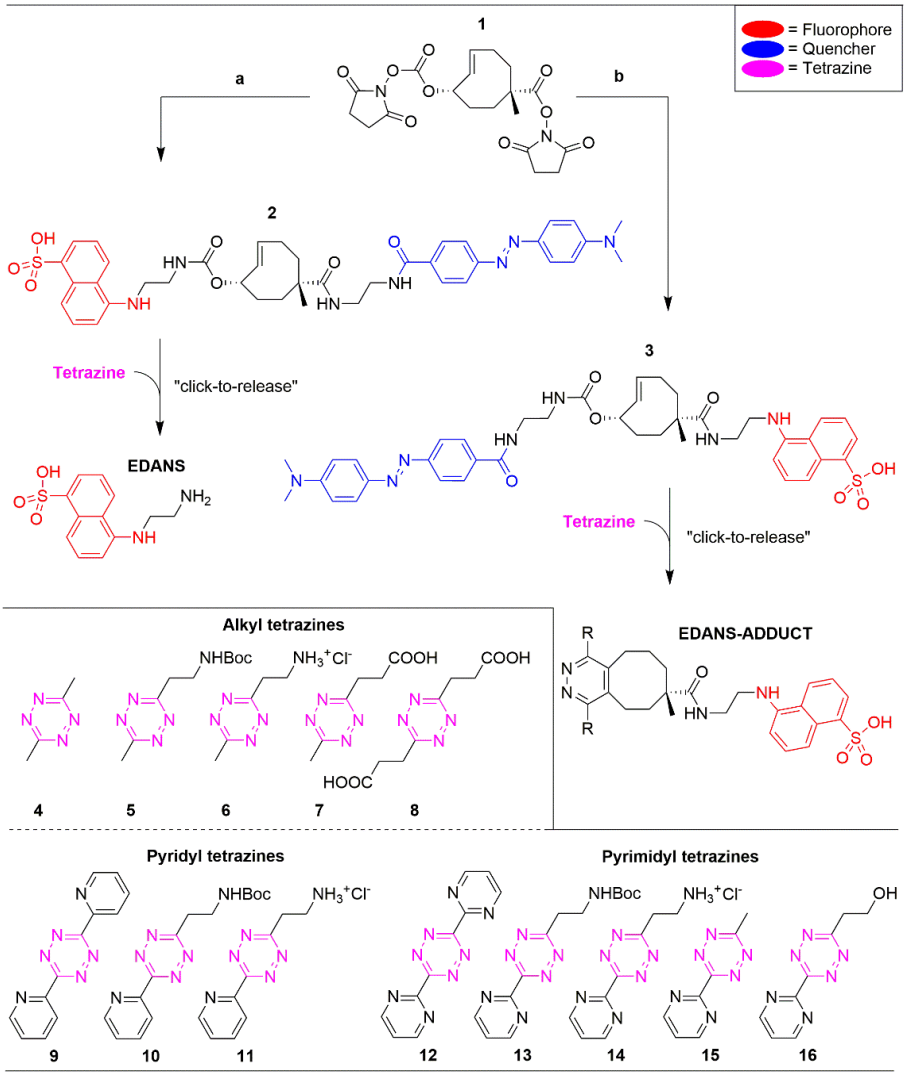

Scheme 1: (**Top**) Functionalization of bifunctional TCO **1** into probes **2** and **3** accompanied with a structure of the fluorescent end-product after reaction with tetrazine and subequent release. (**Bottom**) Previously synthesized tetrazines used in this chapter.

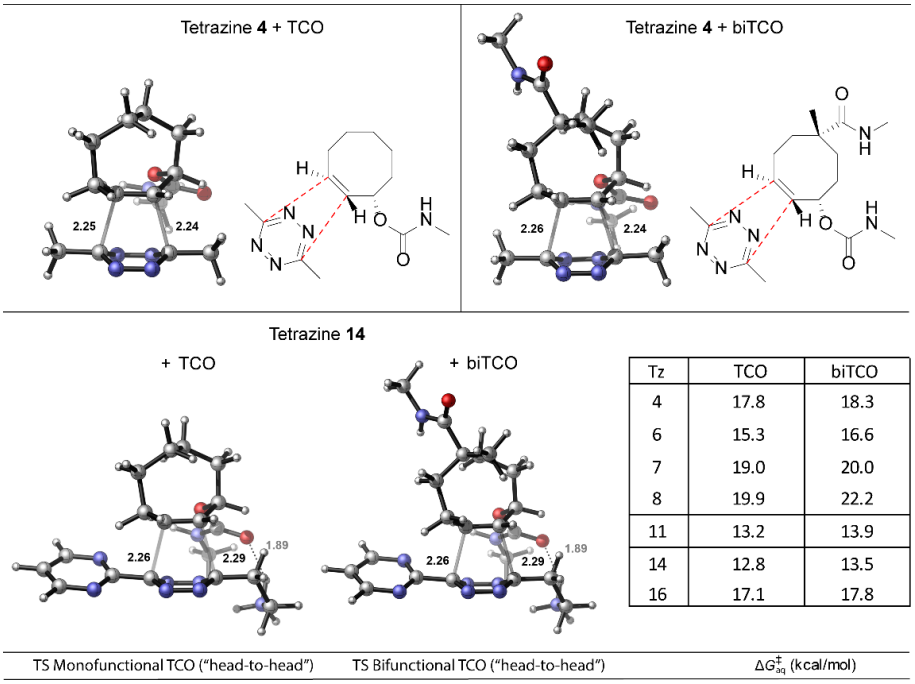

Tz	TCO	biTCO
4	17.8	18.3
6	15.3	16.6
7	19.0	20.0
8	19.9	22.2
11	13.2	13.9
14	12.8	13.5
16	17.1	17.8

Figure 1: "Head-to-head" transition state energies of tetrazines **2**, **6**, **7**, **8**, **11**, **14** and **16** with model mono- or bi-functional axial (E)-cyclooct-2-ene. Distances of interest (forming C-C bonds, interactions) are labelled in Å. Reported transition states were used for initial approximations.[8-9] All generated structures were further optimized with Gaussian using the M06-2X hybrid functional[6] and 6-31+G(d) as basis set. Optimization was done in combination with a polarizable continuum model using water as solvent parameter.

its beneficial interaction with the carbonyl at the TCO's allylic carbamate. The presence of electron withdrawing pyridyl and pyrimidyl functionalities also lowered the TS energy.

Determination of elimination kinetics

Starting from bifunctional TCO **1**, the activated carbonate could be functionalized first, followed by functionalizing the activated ester, to make EDANS releasing fluorogenic probe **2** and DABCYL releasing fluorogenic probe **3**. Next, both constructs were tested in a phosphate buffered solution (0.2M PO_4^{2-} solution in 10% DMSO) to determine the release reaction kinetics in the presence of commonly used tetrazines from literature (alkyl tetrazines **4-8**, pyridyl tetrazines **9-11**, and pyrimidyl tetrazines **12-16**). Initially both probes **2** and **3** were analyzed to determine the elimination behavior of the tetrazines when reacting with bifunctional TCOs. Each of the tetrazines were tested on both probes and for each probe two concentrations were used, either 400 µM (**Figure 2**) or 100 µM (**Figure 3**). The fluorescence emergence

was analyzed until t = 240 minutes, by which time the change in fluorescence had become minimal. To determine the elimination efficiency and reaction rates involved during the reaction, decay trendlines were fitted to the data using ***GraphPad Prism***. Unlike the fluorescence signals observed in **chapter 5**, where the release of coumarin from monofunctional TCO was emerging from a single "eliminating" adduct following a "one-phase exponential decay" trend accompanied with a single reaction rate, the fluorescence signal from the release of alkyl amines from both probe **2** and **3** did not fit a "one-phase exponential decay" trend, with the exception of tetrazine **4**. Alternatively a "two-phase exponential decay" trendline appeared to be

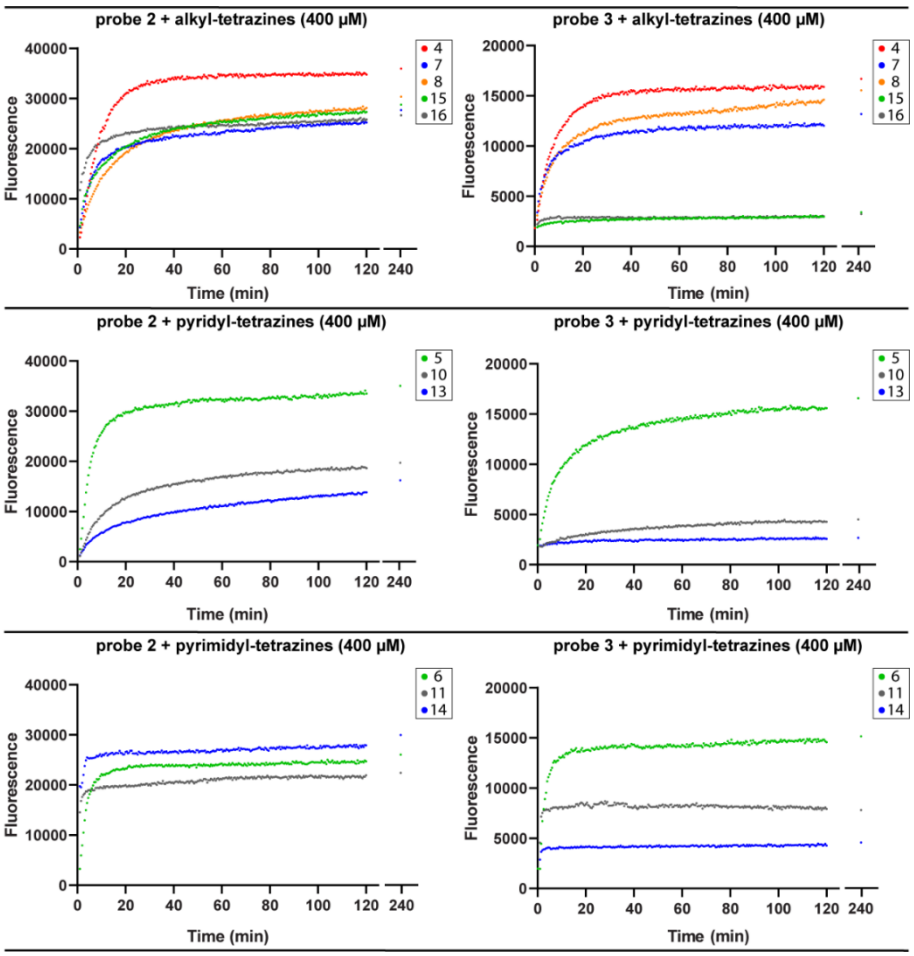

Figure 2: Raw data of the fluorescence emergence when reacting either EDANS releasing probe **2** (left, 10 µM) or DABCYL releasing probe **3** (right, 10 µM) with tetrazines **4** – **8**, **10** – **11** and **13** – **16** (400 µM) measured over a time period of 120 minutes, followed by an additional measurement at 240 minutes.

a near-perfect fit for the fluorescence signals obtained. This suggested that is was likely that when using probe **2** or **3**, having a bifunctional TCO attached to an alkyl amine, at least two measurable eliminating processes existed during the reaction with the tested tetrazines. Similar to what was shown in literature[2], this could be the result from multiple reversible tautomeric intermediates (one non-eliminating and one eliminating) formed from a single IEDDA adduct (**Scheme 2**). When comparing the fluorescence signals obtained from probe **2** and **3** it appeared that the intensity was significantly lower for DABCYL-releasing probe **3** (**Figure 4**).

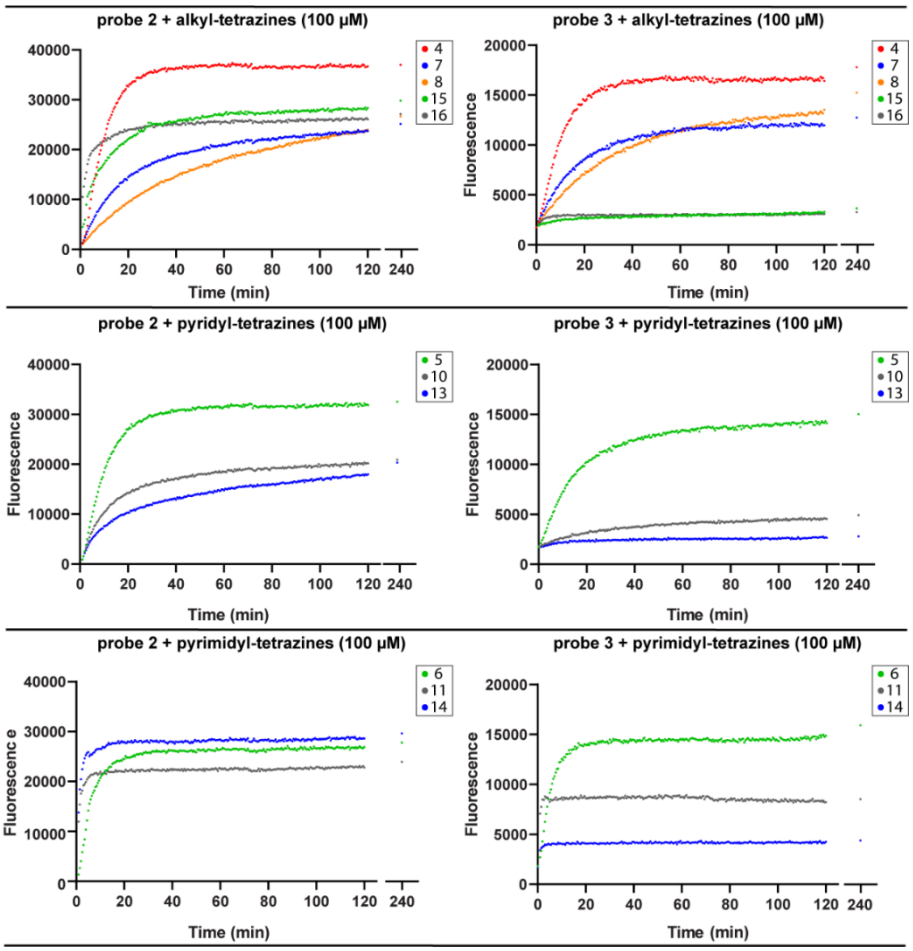

Figure 3: Raw data of the fluorescence emergence when reacting either EDANS releasing probe **2** (left, 10 µM) or DABCYL releasing probe **3** (right, 10 µM) with tetrazines **4** – **8**, **10** – **11** and **13** – **16** (100 µM) measured over a time period of 120 minutes, followed by an additional measurement at 240 minutes.

The likely reason for this difference is residual FRET-quenching occurring from the formed pyridazine moiety in close proximity to the attached EDANS, and appeared to be stronger when pyridyl (65% – 77%) or pyrimidyl (84% – 88%) functionalized compared to solely alkyl (46% – 56%) functionalized (**Scheme 3**). For the most accurate analysis and interpretation of the experiments, data obtained from using probe **2** was used to eliminate any undesired influences from FRET-quenching.

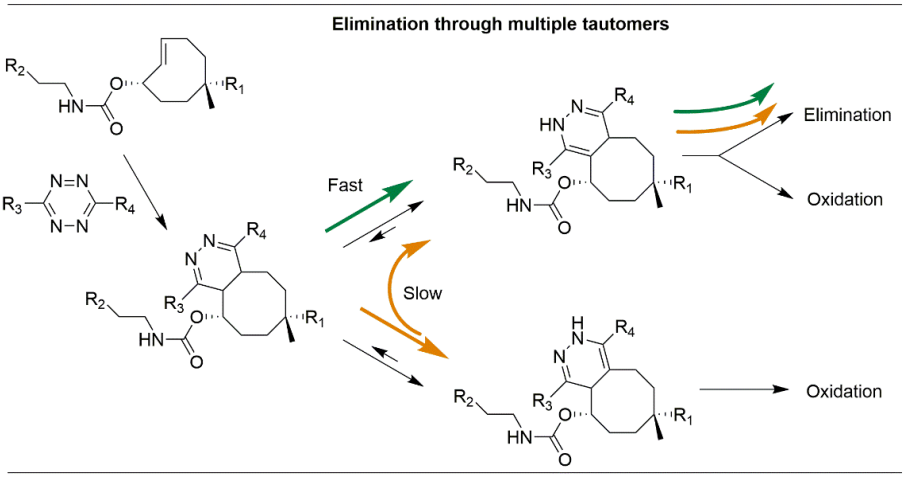

Scheme 2: Proposed mechanism of the "click-to-release" elimination reaction.

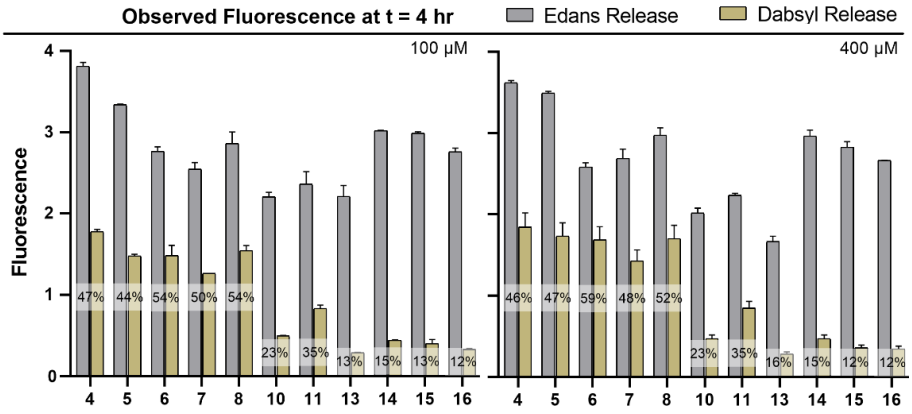

Figure 4: Differences in total amount of fluorescence after 4 hours when using probe **2** (grey) or **3** (yellow).

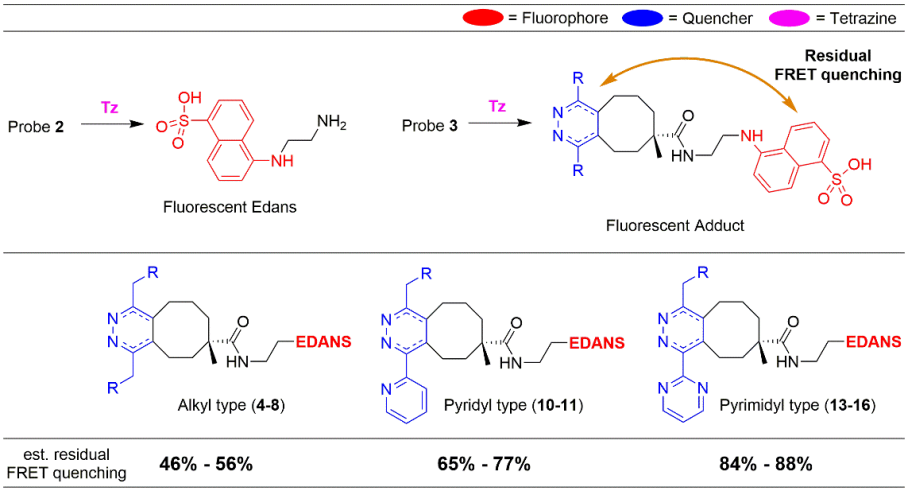

Scheme 3: FRET-quenching from remaining (non-)aromatic pyridazine structures present in close proximity to EDANS when using DABCYL-releasing fluorogenic probe **3**.

After the data was processed (**Figure 5**), for each tetrazine and probe concentration, it provided two reaction rate constants, "k_{fast}" and "k_{slow}", each accompanied with a fractional value describing to what extend they contribute to the total observed fluorescence. These fractional values together represent the elimination efficiency of the entire reaction after 240 minutes normalized to tetrazine **4** which was used as a reference. When looking at the data a whole variety of properties were obtained, where for a select group of tetrazines the tetrazine-specific faster elimination path (k_{fast}) was very dominant. This was observed for hydroxyethyl and aminoethyl tetrazines **6**, **11**, **14** and **16**, indicating a favorable "head-to-head" approach originating from electron-withdrawing substituents, as well as the beneficial intramolecular catalytic effect from the ammonium functionality, as shown in chapter 5, steering towards the eliminating tautomer. Interestingly, for pyridyl and pyrimidyl tetrazines, where the ammonium functionality is absent (tetrazine **15**), or Boc-protected (tetrazines **10** and **13**) the reaction rate constant from the fast elimination path (k_{fast}) is not only reduced by several folds, but the slower elimination path (k_{slow}) appeared to be the favored one as well. Asymmetric carboxylate functionalized tetrazine **8** showed a limited preference for the faster elimination path (k_{fast}) and symmetric carboxylate functionalized tetrazine **9** showed no clearly defined preference for either elimination path.

Tetrazine	[Tz] = 400 µM: Rate constant (K_{obs})	[Tz] = 400 µM: Fraction	[Tz] = 400 µM: Total*	[Tz] = 100 µM: Rate constant (K_{obs})	[Tz] = 100 µM: Fraction	[Tz] = 100 µM: Total*
4	K_{obs} = 20.2 *10^{-4}	**96.5%**	**96.5%**	K_{obs} = 18.9 *10^{-4}	**100%**	**100%**
5	K_{fast} = 43.8 *10^{-4}	74.3%	93.9%	K_{fast} = 17.3 *10^{-4}	83.8%	88.5%
	K_{slow} = 5.7 *10^{-4}	19.6%		**n.d.**	4.7%	
6	K_{fast} = 45.5 *10^{-4}	64.3%	69.8%	K_{fast} = 32.7 *10^{-4}	64.4%	75.5%
	K_{slow} = 1.6 *10^{-4}	5.5%		K_{slow} = 6.1 *10^{-4}	11.1%	
7	K_{fast} = 36.4 *10^{-4}	50.5%	74.6%	K_{fast} = 14.4 *10^{-4}	36.2%	67.7%
	K_{slow} = 3.0 *10^{-4}	24.1%		K_{slow} = 2.9 *10^{-4}	31.5%	
8	K_{fast} = 25.2 *10^{-4}	36.1%	81.5%	K_{fast} = 6.2 *10^{-4}	37.5%	81.0%
	K_{slow} = 4.9 *10^{-4}	45.4%		**n.d.**	33.5%	
10	K_{fast} = 24.4 *10^{-4}	25.9%	61.3%	K_{fast} = 21.9 *10^{-4}	31.3%	55,9%
	K_{slow} = 4.1 *10^{-4}	25.4%		K_{slow} = 4.2 *10^{-4}	24.6%	
11	K_{fast} = 113.7 *10^{-4}	51.4%	59.7%	K_{fast} = 100.2 *10^{-4}	58.1%	63.9%
	K_{slow} = 2.3 *10^{-4}	8.3%		K_{slow} = 2.5 *10^{-4}	5.8%	
13	K_{fast} = 24.5 *10^{-4}	15.6%	41.2%	K_{fast} = 21.6 *10^{-4}	21.1%	56.2%
	K_{slow} = 2.2 *10^{-4}	25.6%		K_{slow} = 2.3 *10^{-4}	35.1%	
14	K_{fast} = 111.0 *10^{-4}	71.7%	81.6%	K_{fast} = 113.3 *10^{-4}	66.0%	79.5%
	K_{slow} = 46.4 *10^{-4}	9.9%		K_{slow} = 14.9 *10^{-4}	13.5%	
15	K_{fast} = 59.0 *10^{-4}	34.1%	77.1%	K_{fast} = 57.7 *10^{-4}	28.7%	79.8%
	K_{slow} = 6.5 *10^{-4}	43.0%		K_{slow} = 8.9 *10^{-4}	51.1%	
16	K_{fast} = 76.4 *10^{-4}	54.1%	72.4%	K_{fast} = 82.2 *10^{-4}	50.4%	73.9%
	K_{slow} = 6.8 *10^{-4}	18.3%		K_{slow} = 9.9 *10^{-4}	23.5%	

*** = Relative to Tetrazine 4**

Figure 5: Two phase decay data obtained from ***GraphPad Prism*** when reacting probe **2** with tetrazines at 400 µM (left) and 100 µM (right) concentrations with a fast decay component (K_{fast}) and a slow decay component (K_{slow}).

Kinetic modeling

Because it remained unknown whether the observed reaction rate constants (k_{fast}, k_{slow}), originating from the slow or fast reaction pathway, were limited by the IEDDA ("k_{IEDDA}") or the elimination ("$k_{release}$") step, a kinetic model of the reaction was built in ***Coach 7***[10] to generate data that would represent a fluorescence signal if the theoretical model and its parameters were true.

To limit the complexity of the model, a reaction was modeled (**Figure 6**) where tetrazine ("Tz", 100 µM or 400 µM) and probe ("TCO", 10 µM) react with each other at reaction rates ("IEDDA_rate", k_{IEDDA} = variable) to form a single eliminating intermediate ("Adduct"), according to the following formula:

$$\mathbf{R_{IEDDA} = k_{IEDDA} * [Tz] * [TCO]}$$

This "Adduct" subsequently would eliminate with a specified elimination rate constant ("Elimination_rate", $k_{release}$ = 20 $*10^{-4}$ s^{-1}) to form released "Product". According to the following formula:

$$\mathbf{R_{release} = k_{release} * [Adduct]}$$

As a result from the kinetic modeling a broad list of data points could be obtained on the changing concentration of "Tz", "TCO", "Adduct" and "Product" (**Figure 7**) during the reaction. From these the "Product" data points would represent a simulated fluorescent signal. The simulated fluorescence signal, similar to an experimentally observed fluorescence signal, could be used to generate a decay trendline using ***GraphPad Prism*** to obtain reaction rate constants ("k_{obs}"). The resulting reaction rate constant "k_{obs}" that ***GraphPad Prism*** calculates when feeding ***Coach 7*** data sets would give an understanding to the relationship between the observed "k_{obs}" (calculated by ***GraphPad Prism***) and the actual rate constants "k_{IEDDA}" and "$k_{release}$" of such a reaction (**Figure 8**).

Based on the results obtained from the kinetic modeling, a ratio between the observed rate constants could be calculated using the following formula:

$$\mathbf{Ratio} = \frac{\mathbf{k_{obs,\,high\,[Tz]}}}{\mathbf{k_{obs,\,low\,[Tz]}}}$$

It appears that when the pseudo first order IEDDA rate constant (k_{IEDDA} * [Tz]) is much larger than the first order elimination rate constant ($k_{release}$), as shown for parameters A, the ratio will remain largely unchanged:

$$\frac{\mathbf{k_{obs,\,high\,[Tz]}}}{\mathbf{k_{obs,\,low\,[Tz]}}} \approx \frac{\mathbf{k_{release}}}{\mathbf{k_{release}}} \approx \mathbf{1}$$

In this situation the rate limiting step is the elimination step, which is independent of the tetrazine concentration. Here the observed rate (k_{obs}) can be used as an approximation of the elimination rate ($k_{release}$).

When the pseudo first order IEDDA rate constant (k_{IEDDA} * [Tz]) is much smaller than the first order elimination rate constant ($k_{release}$), as shown for parameters E, the ratio will be the same as the ratio between both tetrazine concentrations:

$$\frac{k_{obs,\ high\ [Tz]}}{k_{obs,\ low\ [Tz]}} \approx \frac{k_{IEDDA}*[Tz]_{high}}{k_{IEDDA}*[Tz]_{low}} \approx \frac{[Tz]_{high}}{[Tz]_{low}} \approx 4$$

In this situation the rate limiting step is the IEDDA step, which is dependent on the tetrazine concentration. Here, the observed rate (k_{obs}) can be used as an approximation of the pseudo first order IEDDA rate constant (k_{IEDDA} *[Tz]).

Finally, when the pseudo first order IEDDA rate constant (k_{IEDDA} * [Tz]) is similar to the first order elimination rate constant ($k_{release}$), as shown for parameters B, C and D, the ratio will be in between the two values. In this situation both the IEDDA step as well as the elimination step are contributing as a rate limiting step. Here, the observed rate (k_{obs}) can be used to approximate either the rates with a somewhat limited accuracy.

Analysis of experimental results

With the modeling data finished, the experimental data could be analyzed to obtain a ratio for each of the reactions k_{obs}, k_{fast}, or k_{slow}, whenever possible (**Figure 9**). From these ratio values the reaction would be considered limited by IEDDA rate when the ratio was > 3.06, limited by release rate when the ratio was < 1.66, or limited by both when the ratio was inbetween 1.66 and 3.06.

Then for the IEDDA rate limited reactions the rate constant ("k_{IEDDA}") was determined through the following formula using the lower (100 µM) concentration value, as it would provide a better approximation:

$$k_{obs,\ low\ [Tz]} / [Tz]_{low} \approx k_{IEDDA}\ (M^{-1}\ s^{-1})$$

For the release rate limited reactions the rate constant ("$k_{release}$") was determined through the following formula using the lower (400 µM) concentration value, as it would provide a better approximation:

$$k_{obs,\ high\ [Tz]} \approx k_{release}\ (s^{-1})$$

And finally for the in between reaction, both formulas were used to give a rough estimation (> 60%) of each of the rate constants.

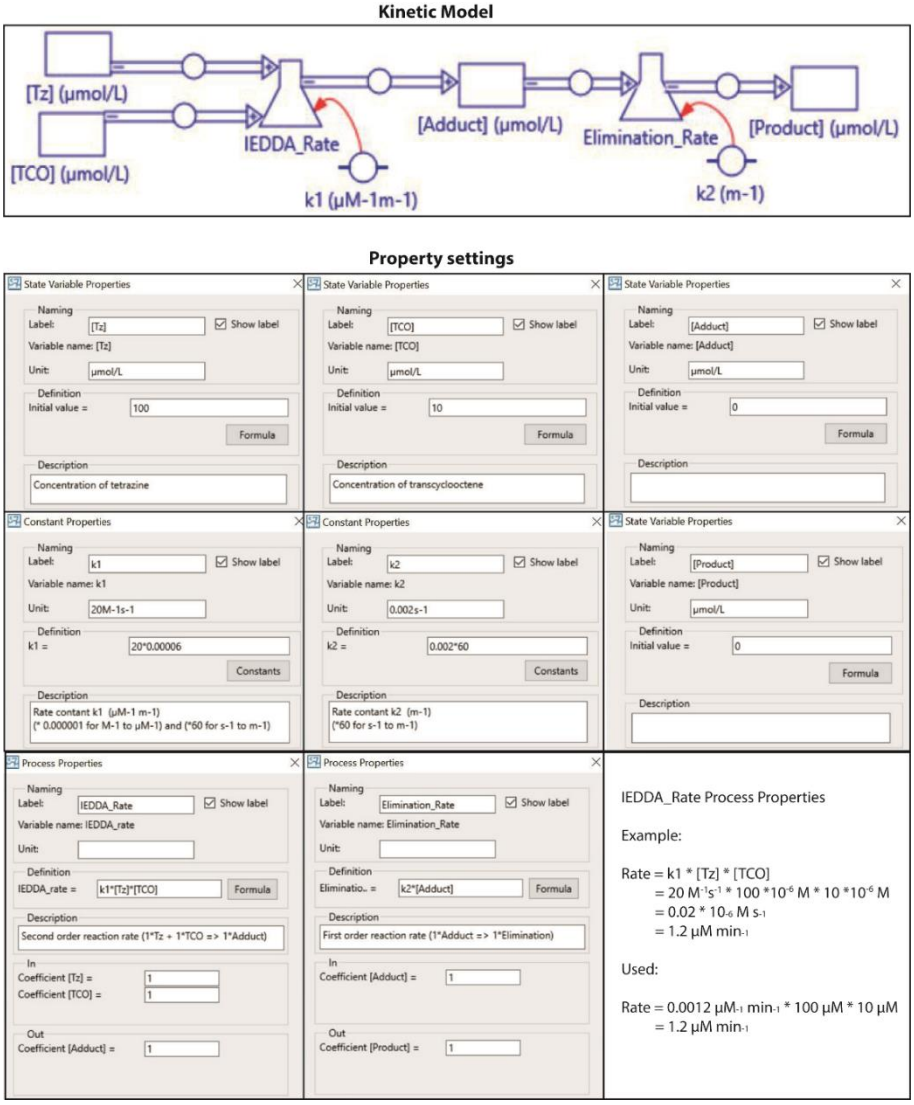

Figure 6: One phase decay click-to-release reaction model using ***Coach 7***.

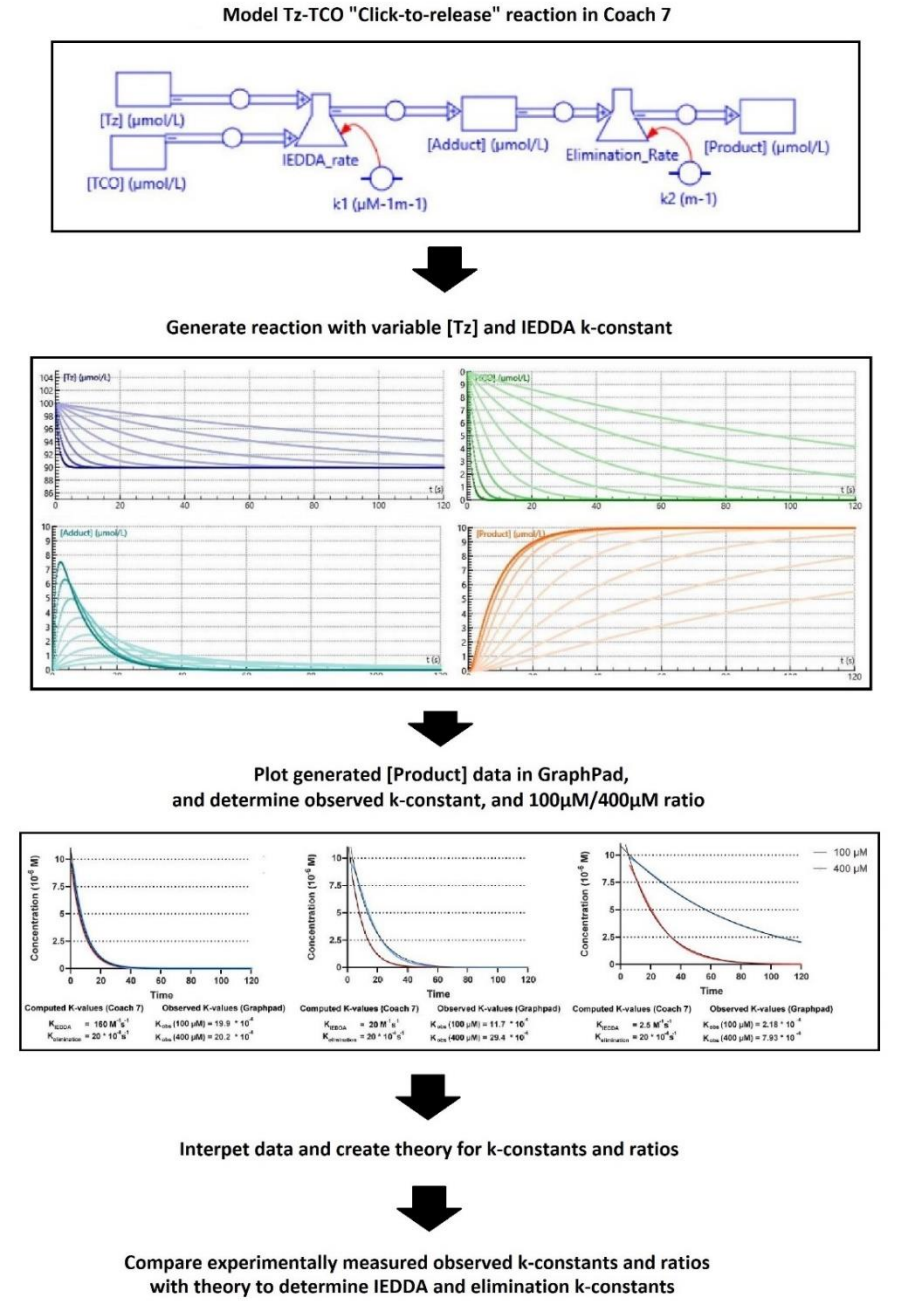

Figure 7: Data generation pathway into understanding the relationship between observed reaction rate "K_{obs}" calculated by *GraphPad Prism* and model reaction "K_{IEDDA}" and elimination "$K_{release}$" rates.

Data interpretation

	Input					Output	
	[TCO]	[Tz]	$K_{release}$	K_{IEDDA}	K_{IEDDA} * [Tz]	K_{obs}	Ratio
	µM		* 10^{-4} s^{-1}	$M^{-1}s^{-1}$	* 10^{-4} s^{-1}	* 10^{-4} s^{-1}	
A	10	100	20	160	160	19.9	1.02
		400			720	20.2	
B	10	100	20	20	20	11.7	1.66
		400			80	19.4	
C	10	100	20	10	10	7.4	2.29
		400			40	17.0	
D	10	100	20	5	5	4.2	3.06
		400			20	12.7	
E	10	100	20	1.25	1.25	1.1	3.96
		400			5.0	4.4	

$$\text{Ratio} = \frac{K_{obs}([Tz] = 400\ \mu M)}{K_{obs}([Tz] = 100\ \mu M)}$$

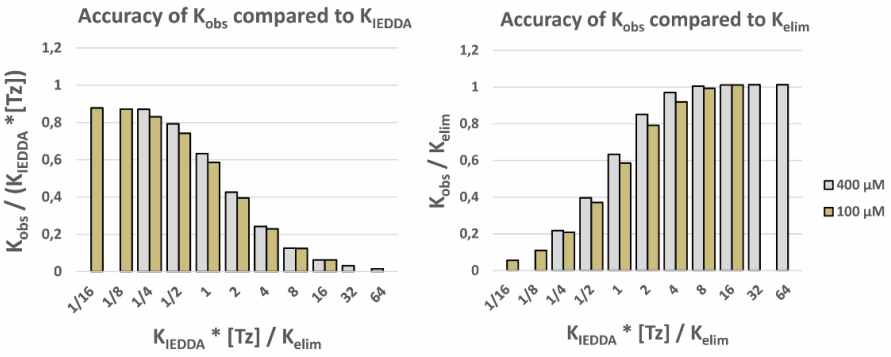

Kobs provides an approximation of KIEDDA when KIEDDA * [Tz] is smaller than Krelease

Kobs provides an approximation of Krelease when KIEDDA * [Tz] is larger than Krelease

Observation	Result	Interpetation
Ratio ≈ 1	k_{obs} is independent of [Tz]	$K_{obs} \approx K_{release}$
Ratio ≈ $[Tz]^{high}$ / $[Tz]^{low}$	k_{obs} is dependent of [Tz]	$K_{obs} \approx K_{IEDDA}$ * [Tz]

Figure 8: Top: Modeling parameters **A**, **B**, **C**, **D** and **E** used in ***Coach 7*** to generate simulated fluorescence signal (**input**) and the observed reaction rate constant K_{obs} obtained in ***GraphPad Prism*** by approximation of the 1st order reaction rate using the simulated fluorescence readout (**output**). **Middle:** A graphical view of how the K_{obs} generated by ***Graphpad Prism*** compares to K_{IEDDA} (left graph) or $K_{release}$ (right graph), and how accurate (closer to 1 is more accurate) this value is. **Bottom:** An explanation of what the observed reaction rate constant K_{obs} approximates to depending on the change fluorescent readout observed when adjusting the tetrazine concentration [Tz] by 4-fold within a single modeling parameter.

				Rate limiting rate constant		Lit. K_{IEDDA}
Tetrazine	Rate constant	Ratio	Rate limiting step	K_{IEDDA} (100 µM, M^{-1} S^{-}	$K_{release}$ (400 µM, s^{-1})	K_{IEDDA} (M^{-1} S^{-1})
4	K_{obs}	1.1	**release**	-	20.2 * 10^{-4}	48.7
5	K_{fast}	2.5	**both**	(est.) 17.3	(est.) 43.8 *10^{-4}	-
	K_{slow}	n.d.	n.d.	-	-	-
6	K_{fast}	1.39	**release**	-	45.5 * 10^{-4}	-
	K_{slow}	n.d.	n.d.	-	-	-
7	K_{fast}	2.5	**both**	(est.) 14.4	(est.) 36.4 *10^{-4}	17.5
	K_{slow}	1.0	**release**	-	3.0 * 10^{-4}	-
8	K_{fast}	4.1	**IEDDA**	6.2	-	6.7
	K_{slow}	n.d.	n.d.	-	-	-
10	K_{fast}	1.1	**release**	-	24.4 * 10^{-4}	-
	K_{slow}	1.0	**release**	-	4.1 * 10^{-4}	-
11	K_{fast}	1.1	**release**	-	113.7 *10^{-4}	-
	K_{slow}	1.5	**release**	-	2.3 * 10^{-4}	-
13	K_{fast}	1.1	**release**	-	24.5 * 10^{-4}	-
	K_{slow}	0.9	**release**	-	2.2 * 10^{-4}	-
14	K_{fast}	1.0	**release**	-	111.0 *10^{-4}	-
	K_{slow}	n.d.	n.d.	-	-	-
15	K_{fast}	1.0	**release**	-	59.0 * 10^{-4}	-
	K_{slow}	0.7	**release**	-	6.5 * 10^{-4}	-
16	K_{fast}	0.9	**release**	-	76.4 *10^{-4}	-
	K_{slow}	0.7	**release**	-	6.8 * 10^{-4}	-

Figure 9: Interpretation of the two phase decay data obtained from ***GraphPad Prism*** when reacting probe **2** with tetrazines at 400 µM and 100 µM concentrations with a fast decay component (K_{fast}) and a slow decay component (K_{slow}). Rate limiting steps comparison of the ratio between the two components, including respective assigned rate limiting rate constant. Known rate constants from literature were added for comparison.

Approximation of K_{IEDDA}

With all the rate constants determined, most of the tetrazines only one of the two rate constants was determined. To be able to find the other rate constant the difference between the (pseudo) first order rate constants k_{IEDDA} * [Tz] and $K_{release}$ must be adjusted towards where the desired reaction step is limiting the observed reaction rate, as shown in the middle graphs of **Figure 8**. The most feasible way to

achieve this is through adjusting the tetrazine concentration. By increasing the tetrazine concentration above the concentrations previously used it may be possible to approximate $K_{release}$ rate constants for tetrazines limited by the IEDDA reaction step, but unfortunately this was not possible in the setup used. On the other side it was possible to approximate the k_{IEDDA} rate constants for tetrazines **4**, **6**, **11** and **14** by lowering the tetrazine concentration to 5-10 µM (**Figure 10**). Unfortunately the concentration of probe **2** also had to be lowered to 100 nM, and as a result lowering the tetrazine concentrations even further resulted in a too slow reaction to yield accurate data.

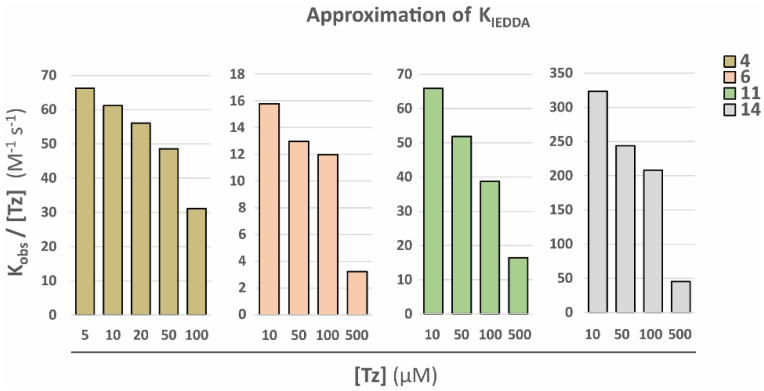

Figure 10: Approximation of K_{IEDDA}, by lowering the tetrazine concentration.

Conclusion

To conclude the chapter, probes **2** and **3** were synthesized successfully and probe **3** appeared to perform poorly due to FRET-quenching by the diazine moiety withing the product. Probe **2** performed well and the fluorescence data obtained allowed the identification of rate constants for multiple eliminating pathways within a single reaction. These rate constants could then, together with obtained knowledge from theoretically modeled data, be used to approximate the IEDDA reaction rate constant (K_{IEDDA}) or multiple eliminating rate constants (k_{fast}, k_{slow}) within a single reaction. Finally it was shown that for reactions where the eliminating reaction step was the rate limiting step, the IEDDA reaction rate constant could be approximated by lowering both the probe and tetrazine concentrations.

Computational Chemistry

Geometry optimization: structures

A conformer distribution search option included in the Spartan 10 program[5] with the use of MM with MMFF94 as force field, was used as starting point for the geometry optimization. All generated structures were further optimized with Gaussian 09 using the M06-2X hybrid functional[6] and 6-31+G(d) as basis set. Optimization was done in gas-phase and subsequently corrections for solvent effects were done by the use of a polarizable continuum model using water as solvent parameter. The denoted free Gibbs energy was calculated using Equation (1), in which ΔE_{gas} is the gas-phase energy (electronic energy), $\Delta G^{T}_{gas,QH}$ (T = 293.15 K and pressure = 1 atm.) is the sum of corrections from the electronic energy to the free Gibbs energy in the quasi-harmonic oscillator approximation, including zero-point-vibrational energy, and ΔG_{solv} is their corresponding free solvation Gibbs energy. The $\Delta G^{T}_{gas,QH}$ were computed using the quasi-harmonic approximation in the gas phase according to the work of Truhlar - the quasi-harmonic approximation is the same as the harmonic oscillator approximation except that vibrational frequencies lower than 100 cm^{-1} were raised to 100 cm^{-1} as a way to correct for the breakdown of the harmonic oscillator model for the free energies of low-frequency vibrational modes.[7] Visualization of relevant structures was done with CYLview. All denoted distances are expressed in ångström (Å).

$$\Delta G^{T}_{aq} = \Delta E_{gas} + \Delta G^{T}_{gas,QH} + \Delta G_{solv} \quad (1)$$

$$= \Delta G^{T}_{gas} + \Delta G_{solv}$$

Geometry optimization: IEDDA transition state structures

Initial guesses for the transition states were based on the work of Fox and co-workers[8] and Houk and co-workers.[9] All generated structures were further optimized with Gaussian using the M06-2X hybrid functional and 6-31+G(d) as basis set. Optimization was done in combination with a polarizable continuum model using water as solvent parameter.

Compound Synthesis

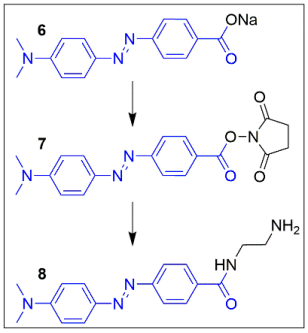

Compound 8: 0.50 mmol (145 mg) of commercially available DABCYL sodium carboxylate **6** (0.145 g, 0.50 mmol) was dissolved in 8.8 mL dry DMF. Then 0.66 mmol (76.5 mg) of N-hydroxy succinimide and 1.00 mmol (193 mg) of EDC*HCl were added and the reaction mixture was stirred overnight at room temperature. The resulting mixture was concentrated using rotary evaporation and purified with silica column chromatography over silica gel using a 0-2% MeOH in DCM eluent resulting in 169 mg (0.46 mmol, 96%) of intermediate **7**. Intermediate **7** was then dissolved in 11 mL of dry DMF, 60 mmol (4 mL) of ethylenediamine and 0.57 mmol (100 µL) of TEA were added and the reaction mixture was stirred overnight at room temperature. The resulting mixture was concentrated using rotary evaporation and purified with silica column chromatography over silica gel using a 10-20% MeOH in DCM eluent resulting in 134 mg (0.43 mmol, 93%) of compound **8**. ^{1}H NMR (400 MHz, $CDCl_3$) δ: 8.30 – 8.23 (m, 2H), 8.10 (s, 2H), 8.03 (d, 2H), 6.89 (d, 2H), 3.22 (s, 6H), 3.00 – 2.90 (m, 4H). HRMS (m/z): $[C_{17}H_{21}N_5O + H]^+$ calculated 312.1819, found 312.1817.

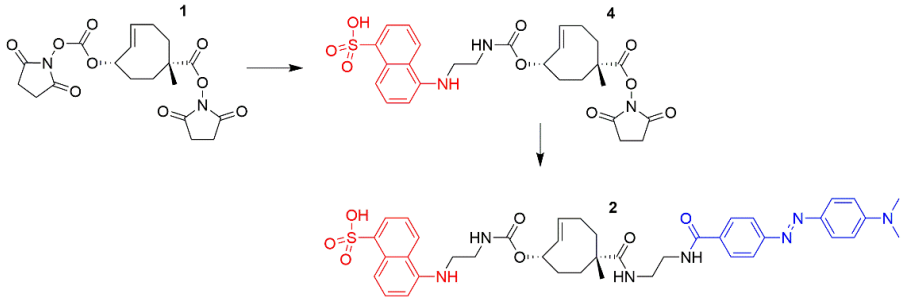

Compound 2: 57 µmol (15 mg) of commercially available 1,5-EDANS and 47 µmol (20 mg) of compound **1** were added to a 2 mL Eppendorf tube. Then, 1 mL of dry DMF and 5 equivalents of TEA were added and the Eppendorf tube was shaken overnight in the dark (wrapped in aluminum foil). The resulting mixture was concentrated using rotary evaporation and purified with silica column chromatography using a MeOH in DCM eluent resulting in 21 mg (37 µmol, 79%) of intermediate **4.** Then, 10 µmol (4.9 mg) of intermediate **4** and 11 µmol (3.4 mg) of compound **8** were added to a 2 mL Eppendorf tube. Then, 1 mL of dry DMF and 5 equivalents of TEA were added and the Eppendorf tube was shaken overnight in the dark (wrapped in aluminum foil). The resulting mixture was concentrated using rotary evaporation and purified with silica column chromatography using a MeOH in DCM eluent resulting in 4.8 mg (6.2 µmol, 62%) of compound **2** as a red solid. ***Intermediate 4***: ^{1}H NMR (500 MHz, MeOD) δ: 8.14 (m), 7.45 – 7.32 (m), 6.74 – 6.61 (m), 5.92 (m), 5.70 (m), 3.82 (m), 3.64 – 3.56 (m), 3.53 (m), 3.49 (m), 3.38 (m), 3.09 (m), 2.82 – 2.76 (m), 2.52 (m), 2.30 – 2.22 (m), 1.28 (m). ^{13}C NMR (126 MHz,

MeOD) δ: 175.89, 175.36, 171.89, 145.48, 145.43, 141.75, 133.25, 132.10, 131.39, 130.95, 128.58, 128.52, 126.68, 125.62, 125.58, 125.50, 125.41, 123.58, 116.26, 115.40, 105.06, 73.48, 56.81, 55.77, 45.63, 45.29, 44.73, 43.76, 40.76, 39.71, 39.65, 36.63, 31.65, 31.55, 31.28, 28.80, 26.48, 26.34, 26.21, 18.47, 13.16. ***Compound 2***: ^{1}H NMR (500 MHz, MeOD) δ: 8.00 – 7.80 (m), 6.74 (m), 5.88 (m), 5.58 (m), 5.14 (m), 5.09 (m), 3.66 (s), 3.61 (m), 3.47 (m), 3.09 (s), 2.95 (s), 2.87 (s), 2.80 (m), 2.57 (m), 2.24 (m), 2.05 (m), 1.89 (m), 1.24 (m), 1.12 (m). HRMS (m/z): $[C_{40}H_{47}N_7O_7S + H]^+$ calculated 770.3330, found 770.3320.

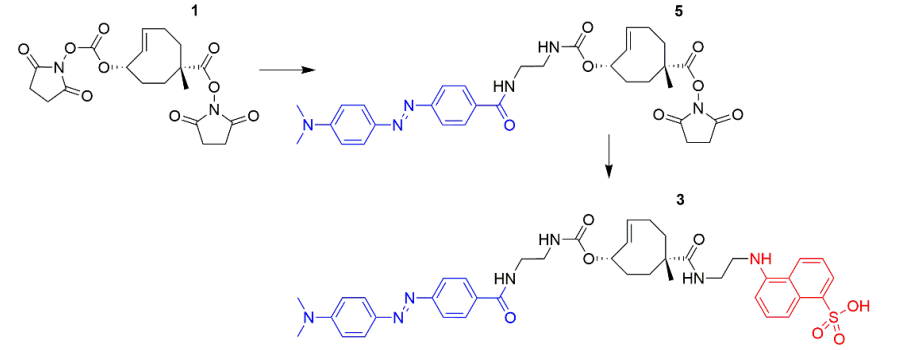

Compound 3: 29 µmol (9.0 mg) of compound **8** and 30 µmol (13 mg) of compound **1** were added to a 2 mL Eppendorf tube. Then, 1 mL of dry DMF and 5 equivalents of TEA were added and the Eppendorf tube was shaken overnight in the dark (wrapped in aluminum foil). The resulting mixture was concentrated using rotary evaporation and purified with silica column chromatography using a MeOH in DCM eluent resulting in 21 mg (28 µmol, 96%) of intermediate **5**. Then, 5.2 µmol (3.2 mg) of intermediate **5** and 5.5 µmol (1.6 mg) of commercially available 1,5-EDANS were added to a 2 mL Eppendorf tube. Then, 1 mL of dry DMF and 5 equivalents of TEA were added and the Eppendorf tube was shaken overnight in the dark (wrapped in aluminum foil). The resulting mixture was concentrated using rotary evaporation and purified with silica column chromatography using a MeOH in DCM eluent resulting in 3.6 mg (4.6 µmol, 88%) of compound **3**. ***Intermediate 5***: ^{1}H NMR (500 MHz, $CDCL_3$) δ: 8.01 (s), 7.95 – 7.86 (m), 7.85 (d, *J* = 8.6 Hz), 7.73 (dd, *J* = 8.9, 0.7 Hz), 7.48 (dd, *J* = 1.9, 0.8 Hz), 7.22 (dd, *J* = 8.9, 1.8 Hz), 6.76 (d, *J* = 9.1 Hz), 5.92 – 5.82 (m), 5.65 – 5.55 (m), 5.18 (s), 3.75 – 3.60 (m), 3.50 (m), 3.25 – 3.00 (m), 2.96 (s), 2.88 (s), 2.81 (m), 2.27 (m), 2.04 (m), 1.91 (m), 1.40 – 1.34 (m), 1.33 – 1.22 (m). ^{13}C NMR (126 MHz, $CDCl_3$) δ: 174.4, 167.8, 157.1, 155.2, 152.9, 143.7, 141.6, 134.1, 132.1, 131.7, 131.3, 128.6, 128.1, 125.7, 125.5, 122.3, 119.7, 111.6, 110.1, 72.5, 67.2, 54.2, 46.3, 44.5, 44.4, 42.5, 41.6, 40.8, 40.4, 36.6, 35.9, 31.6, 30.6, 30.5, 29.8, 25.7, 18.7, 18.0, 17.6, 12.2, 8.8. ***Compound 3***: ^{1}H NMR (500 MHz, MeOD) δ: 8.13 (m), 7.92 (m), 7.85 (m), 7.37 (m), 6.79 (m), 6.66 (m), 5.89 (m), 5.65 (m), 3.60 – 3.35 (m), 3.20 – 3.00 (m), 2.19 (m), 2.07 (m), 1.90 (m), 1.71 (m), 1.61 (m), 1.47 (m), 1.29 (m), 1.11 (m), 0.89 (m). HRMS (m/z): $[C_{40}H_{47}N_7O_7S + H]^+$ calculated 770.3330, found 770.3321.

References

[1] X. Fan, Y. Ge, F. Lin, Y. Yang, G. Zhang, W.S.C. Ngai, Z. Lin, S. Zheng, J. Wang, J. Zhao, J. Lie, P.R. Chen, *Angew. Chem. Intl. Ed.*, **2016**, 55, 14046-14050.

[2] J.C.T. Carlson, H. Mikula, R. Weissleder, *J. Am. Chem. Soc.*, **2108**, 140, 3603-3612.

[3] A.J.C. Sarris, T. Hansen, M.A.R. de Geus, E. Maurits, W. Doelman, H.S. Overkleeft, J.D.C. Codée, D.V. Filippov, S.I. van Kasteren, *Chem. Eur. J.*, **2018**, 24, 1-8.

[4] R. Rossin, S.M.J. van Duijnhoven, W. ten Hoeve, H.M. Janssen, L.H.J. Kleijn, F.J.M. Hoeben, R.M. Versteegen, M.S. Robillard, *Bioconjugate Chem.*, **2016**, 27, 1697-1706.

[5] Y. Shao, L. F. Molnar, Y. Jung, J. Kussmann, C. Ochsenfeld, S. T. Brown, A. T. B. Gilbert, L. V Slipchenko, S. V Levchenko, D. P. O'Neill, et al., *Phys. Chem. Chem. Phys.* **2006**, *8*, 3172–3191.

[6] A. V. Marenich, C. J. Cramer, D. G. Truhlar, *J. Phys. Chem. B* **2009**, *113*, 6378–6396.

[7] R. F. Ribeiro, A. V. Marenich, C. J. Cramer, D. G. Truhlar, *J. Phys. Chem. B* **2011**, *115*, 14556–14562.

[8] M. T. Taylor, M. L. Blackman, O. Dmitrenko, J. M. Fox, T. Ligation, *J. Am. Chem. Soc.* **2011**, *133*, 9646–9649.

[9] F. Liu, Y. Liang, K. N. Houk, *J. Am. Chem. Soc.* **2014**, *136*, 11483–11493.

[10] Coach 7. version 7.6.001. (https://cma-science.nl/)